Microstructure and thermomechanical characteristics of spark plasma sintered TiC ceramics doped with nano-sized WC

Abbas Sabahi Namini, Zohre Ahmadi, Aziz Babapoor, Mohammadreza Shokouhimehr, Mehdi Shahedi Asl

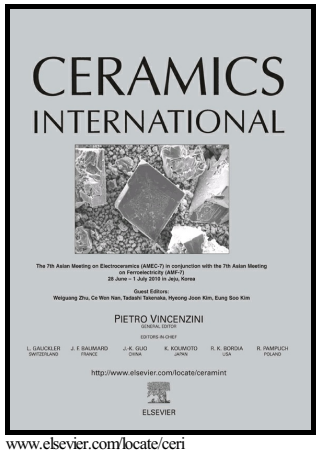

www.elsevier.com/locate/ceri

PII: S0272-8842(18)32929-8
DOI: https://doi.org/10.1016/j.ceramint.2018.10.125
Reference: CERI19837

To appear in: *Ceramics International*

Received date: 3 October 2018
Revised date: 15 October 2018
Accepted date: 15 October 2018

Cite this article as: Abbas Sabahi Namini, Zohre Ahmadi, Aziz Babapoor, Mohammadreza Shokouhimehr and Mehdi Shahedi Asl, Microstructure and thermomechanical characteristics of spark plasma sintered TiC ceramics doped with nano-sized WC, *Ceramics International,* https://doi.org/10.1016/j.ceramint.2018.10.125

Microstructure and thermomechanical characteristics of spark plasma sintered TiC ceramics doped with nano-sized WC

Abbas Sabahi Namini [a,b], Zohre Ahmadi [c], Aziz Babapoor [d], Mohammadreza Shokouhimehr [e], Mehdi Shahedi Asl [c*]

[a] *Department of Advanced Technologies, University of Mohaghegh Ardabili, Namin, Iran.*

[b] *Department of Engineering Sciences, Sabalan University of Advanced Technologies (SUAT), Namin, Iran.*

[c] *Department of Mechanical Engineering, University of Mohaghegh Ardabili, Ardabil, Iran.*

[d] *Department of Chemical Engineering, University of Mohaghegh Ardabili, Ardabil, Iran.*

[e] *Department of Materials Science and Engineering, Seoul National University, Seoul 08826, Republic of Korea.*

** Corresponding author: M. Shahedi Asl (shahedi@uma.ac.ir)*

Abstract

In this study, we studied the effects of nano-sized WC addition (0, 1.5 and 3 wt%) on microstructure and thermomechanical properties of TiC-based ceramics. WC-doped TiC matrix composites were sintered by spark plasma at 1900 ˚C under 40 MPa for 7 min. The densification behavior of WC-doped TiC ceramics was characterized and compared with the monolithic TiC. Microstructural investigation of the sintered specimens was achieved by scanning electron microscopy. X-ray diffraction analysis was carried out to determine the phase evolution of the prepared ceramics. In addition, the thermal and mechanical characteristics including thermal conductivity, Vickers hardness and flexural strength were evaluated and their relationship with the microstructural features was discussed. Thermal conductivity increment and the relevant pronounced effects on grain growth inhibition were observed for TiC-3 wt% WC. The obtained results demonstrated that the addition of 3 wt% WC plays a vital role in sinterability enhancement of TiC by accelerating the densification. The highest relative density (99.9 %), Vickers hardness (28.6 GPa) and flexural strength (620 MPa) were obtained for the TiC ceramic doped with 3 wt% nano-sized WC.

Keywords: Titanium carbide; Spark plasma sintering; Tungsten carbide; Microstructure; Thermomechanical characteristics.

1. Introduction

Titanium carbide with special properties has been used for the fabrication of the engineered ceramic components because of its excellent wear resistance, high melting temperature (3250 ˚C), high hardness (> 30 GPa), relatively low density and high resistance to thermal deformation. These characteristics nominates titanium carbide as an important candidate for cutting tools and machining materials [1-6]. However, one of the critical concerns of titanium carbide based ceramics in high stress condition is their low fracture toughness (3.2–3.9 MPa $m^{1/2}$) [7-8]. TiC is very difficult to be sintered by conventional methods due to its strong covalent bonds and high melting temperature [9]. Therefore, it is required to provide huge amount of thermal energy by rising sintering temperature to increase mass transport rate and obtain highly dense products [3, 9]. High temperature and longtime heating treatment, however, leads to grain growth effecting the properties of the obtained ceramics and sintering process [10-12]. To overcome this problem, spark plasma sintering (SPS) has been used to reach fine microstructure materials with high relative density [13-17]. Ishigaki *et al.* could prepare TiC–25 vol% Al_2O_3 by pressureless sintering at 1800 °C having ~80% theoretical density [18]. In contrast, Teber and his coworkers showed that the SPS of mechanical alloyed TiC powder at 1650 °C under 100 MPa, does not produce ceramics with the density of more than 98% [13]. In another study, Cheng *et al*. [9] processed micro-sized TiC powder by SPS technique under conditions of 1600 °C / 50 MPa. Similarly, Cabrero *et al*. [19] fabricated nano-sized TiC powder at 1800 °C under 75 MPa pressure and attained the relative density of 95.7% and 95.4%, respectively. These investigations confirmed that performing the sintering process at higher temperature of 1800 °C and decreasing the particle size of TiC powder cannot result in a completely dense structure [9, 19]. Consequently, sintering aids such as ZrC, TiB_2, SiC and Al_2O_3 can be used as reinforcement materials for titanium carbide based composites lowering the sintering temperature and promoting the densification of TiC powder [20-22]. In addition, it is shown that the dispersion of such ceramic reinforcements into matrix inhibits the growth of TiC grain and result in superior properties [10]. From this point of view, some carbide additives *e.g*. WC, VC, NbC and TaC can be used to decrease the growth rate of TiC grains during sintering and improve mechanical behavior of TiC based composites. Among these additives, WC as one of the most widely used carbide materials with a high melting point (2870 °C) and high Vickers hardness (~22 GPa) can be considered as an appropriate reinforcement material to enhance the sinterability of TiC ceramics [23-32]. Although several attempts have been done on the processing routes and characterization of TiC based composites prepared by SPS, a few investigations have focused on the properties

of binderless TiC–WC composites [24, 25]. Cheng *et al*. fabricated TiC matrix composite reinforced with 3.5 wt% WC by SPS at 1450 °C for 5 min under 50 MPa and attained a relative density of 98.2%, and by comparing with monolithic TiC which sintered under the similar process. The addition of WC as reinforcement reduced the densification temperature for ~150 °C [25]. This finding also showed that it is possible to achieve a complete dense structure by sintering the TiC–3.5 wt% WC at 1600 °C [25]. Furthermore, compared with micro-sized particles, the nano-sized WC powder with higher specific surface areas can be used as reinforcement material to ameliorate the properties of the TiC ceramic [23]. Herein, the aim of this work is to provide a detailed study of the nano-sized WC particles effect on the densification, thermal and mechanical characteristics of TiC matrix composites, combined with deep understanding of their microstructural evolution. In this perspective, the analyses were performed on monolithic TiC and TiC–WC ceramics fabricated by spark plasma sintering, as a modern manufacturing technology [33-50] compared to the other sintering routes [51-61], at 1900 °C for 7 min under 40 MPa. The role of WC on density, grain size variation, hardness and toughening mechanisms was also investigated.

2. Experimental procedure

The specimens used in this study were manufactured from commercial powders, including TiC (average particle size of ~10 μm) and WC (average particle size of ~200 nm). In this study three groups of powder mixtures were designed as shown in Table 1.

The TiC and WC powders were weighed and mixed according to their composition design. Then, the powders were dispersed in ethanol for 20 min using an ultrasonic stirrer. The slurry was mixed for 60 min at 90 rpm using zirconia cup/balls as milling tools. The prepared slurries were heated in a rotating evaporator at 120 ^{o}C to remove the ethanol, crushed and sieved through a mesh of 100 to minimize the particles agglomeration and obtain uniform granules. The dried powder was poured into a graphite die lined with double layer of flexible graphite foils to prevent reaction of the die with the powders. The sintering processes were done by a SPS furnace which was carried out at 1900 °C for 7 min under 40 MPa. During the sintering process, the temperature of the samples was measured by focusing of an optical pyrometer onto the side hole of the graphite die. Finally, the temperature was reduced and the samples with the diameter of 30 mm were removed from instrument.

The surfaces of processed specimens were grinded to remove the graphite foil. The bulk density of the obtained samples was measured through the Archimedes principle, and then the

relative density was estimated by considering the theoretical of the starting powders. Identification of crystalline phases was accomplished by X-ray powder diffraction (XRD, Philips PW3710), and field emission scanning electron microscope (FESEM, Tescan S8000) equipped with energy-dispersive X-ray (EDS) to determine the microstructural features and qualitative chemical composition analyses. The Vickers hardness of the samples was determined through applying the load of 49 N on the polished surface of the sintered materials. The hardness values were considered as average of five indentation measurements. The three-point bending strength was measured at room temperature using a universal testing machine (STM-250) on rectangular polished samples with dimensions of 3 mm × 4 mm × 28 mm and a span length of 15 mm. The thermal conductivity of the sintered samples was calculated using a conductivity meter machine (Sahand Co., Iran) which works with accuracy of ± 3% [62-64]. The average grain size of fabricated specimens was determined using ImageJ software by considering the fracture surface micrographs.

3. Results and discussion

According to the previously published results investigated by Sabahi *et al*., it has been shown that the highest properties for the relevant ceramics can be obtained at the sintering temperature of 1900 ˚C [62]. Hence, in this work the effects of WC additive at the optimal SPS conditions have been investigated. We first characterized the as-prepared powders by SEM and EDS as shown in Fig. 1.

Fig. 1. SEM micrographs and EDS spectra of starting materials: (a) TiC and (b) WC.

The relative density dependence of the TiC-WC composites on WC content is shown in Fig. 2. According to the obtained results, the monolithic TiC reached 99.23% densification of the theoretical density. However, the maximum relative density of 99.85% was attained at WC content of 3 wt%. In contrast, the addition of 1.5 wt% WC to TiC leads to lower densification (93.05% relative density). This results indicate that a higher quantity of WC (3 wt%) exhibits a better effect on densification, which can be attributed to the dissolution and precipitation of WC on TiC grains and formation of (Ti,W)C phase in microstructure of titanium carbide matrix [27-29] facilitating transgranular diffusion causing high rate of the material transfer during sintering. In addition, one of the reasons for the high densification during SPS is the

combined impacts of joule heating, applied pressure and simultaneously local plastic deformation of grains. As can be seen in the FESEM images (Fig. 7), it seems that incorporating 1.5 wt% WC in titanium carbide matrix has a significant effect on the fragmentation of TiC particles and inhibition of grain growth. However, due to the inadequate amount of WC reinforcement, short sintering time, and lack of sufficient time for the elimination of remained porosity, a full condensation of the sample cannot be achieved. Whereas, reinforcing TiC by 1.5 wt% WC and subsequently formation of sufficient amount of solid solution (Ti,W)C contributes to the increased densification percentage and formation of relatively dense material.

Fig. 2. Relative density of TiC containing different amounts of nano-sized WC.

To understand the role of WC reinforcement on densification, consolidation of the specimens was analyzed according to upper punch displacement throughout sintering process, *i.e*. from shrinkage profiles. Fig. 3 illustrates the temperature variation and punch displacement as a function of heating time during SPS. The displacement was affected by the pressure and the temperature. The temperature is gradually increased from 20 to 1900 °C, and the initial pressure of 20 MPa was applied for 8 min and then raised to 50 MPa. In fact, during the first 45 min, the displacement is insignificant and then increases to 1.5, 1.3 and 3.2 mm for TW0, TW1.5 and TW3, respectively, by reaching the temperature to 1800 °C. Therefore, the applied temperature less than 1800 °C is too low to have remarkable effect on densification of monolithic TiC powder. The increase of displacement at temperatures higher than 1800 °C is attributed to various factors such as particle rearrangement, thermal softening of formed grains, and matter flow in the intergranular space. It seems that, the reason for the highest shrinkage value (punch displacement) of TiC-3 wt% WC, compared to the TW0 and TW1.5 compact powders, is the dissolution of tungsten carbide in titanium carbide [23-31] and increasing amount of mass transfer which results in the increased plasticity of the formed grains and elimination of the remained pores in microstructure.

Fig. 3. Variations of displacement and temperature versus dwell time during SPS of TiC-(0, 1.5, 3 wt%) WC ceramics.

Vickers hardness tests were carried out on polished surfaces of sintered samples and the obtained values were displayed as a function of the WC content as shown in Fig. 4. It is observed that the hardness changes in a similar trend to the densification. The hardness of monolithic TiC reduced by incorporating 1.5 wt% WC, but enhanced with increasing the content of WC from 1.5 to 3 wt%. The former is due to the porosity increases in microstructure and the latter is attributed to the formation of (Ti,W)C solid solution [24-28] with higher hardness and the higher relative density. The hardness of these samples is a complex function of composition, relative density and grain size. Therefore, TW3 sample with fine grain size possesses higher hardness than TW0 and TW1.5, which is caused by Hall-Petch hardening effect. As a comparison, Xie *et al*. reported a Vickers hardness of 29 GPa for the monolithic TiC which SPSed under the condition of 1600 ˚C / 5 min / 50 MPa [1]. As it is shown in Fig. 5, the flexural strength of pure TiC was deteriorated from 545 to 418 MPa with 1.5 wt% of WC addition. With further addition of WC content from 1.5 to 3 wt%, the porosity of the sintered sample drastically decreased, accompanied by grain refinement leading to flexural strength improvement from 418 to 620 MPa. Cheng *et al*. reported that TiC based composites containing 3.5 wt% tungsten carbide SPSed at 1600 ˚C could possess densification percentage of 98.4% and flexural strength of 600 MPa [25].

Fig. 4. Vickers hardness of TiC-based ceramics versus the amount of nano-sized WC reinforcement.

Fig. 5. Flexural strength of TiC-based ceramics versus the amount of nano-sized WC reinforcement.

The evolutions of thermal conductivity in the samples reinforced with different amounts of WC are presented in Fig. 6. It is noteworthy that, with the introduction of WC, contradictory effect on thermal conductivity is observed. The finer grain size of TW3 with greater amount of grain boundaries than TW0 should result in lower thermal conductivity. Therefore, it can be assumed that in TW3 sample the effect of chemical composition on thermal properties is greater than the effect of microstructural properties on it. However, as WC has a higher thermal conductivity than TiC at room temperature, the introduction of 3 wt% WC causes increment of thermal conductivity from 17.7 W/m K (for TW0) to 21.13 W/m K (for TW3). But, the thermal conductivity of TW1.5 is 14.22 W/m K, which is 20% lower than the thermal conductivity of TW0. This decrement indicates minor thermal distribution in TW1.5 which is occurred as a result of 7% porosity in this sample.

Fig. 6. Thermal conductivity of TiC-based ceramics versus the amount of nano-sized WC addition.

The FESEM images of the polished and fracture surfaces of the processed specimens are presented in Fig. 7. As can be observed in Fig 7a, the sintering phenomena proceeds by adhesion and bond formation between TiC particles. As compared with raw TiC particle size, a slight grain growth was happened during sintering of monolithic TiC, which means that such sintering condition leads to a small growth of TiC grain size. According to Fig. 7a, it is possible to fabricate an approximately fully dense TiC ceramic with no addition of WC reinforcement in the starting powder. However, slight densification development can be occurred after adding 3 wt% WC. The porosity content increased to ~7% by addition of 1.5 wt% WC to TiC as clearly observable in Fig 7b. According to the microstructure of TW3 sample shown in Fig. 7c, almost no porosity remained in this sample which is in agreement with the obtained result of 99.85% relative density for TW3. In addition, precise observation of FESEM images reveals multiple mode of fractures in the monolithic TiC. However, on the reinforcement with 3 wt% WC, the fracture behavior changes from a primarily transgranular for TW0 sample to a predominantly intergranular mode for TW3 sample.

Fig. 7. FESEM images of the polished and fracture surfaces of nano-sized WC-doped TiC ceramics: (a) TW0, (b) TW1.5 and (c) TW3.

By considering the fracture surface micrographs through the imaging analysis technique, the average grain size for sintered materials was obtained (Fig. 8), which indicates reduction in the grain size by adding WC. The grain size of TiC matrix in TW3 sintered sample is ~7.3 μm as compared to the mean grain size of additive-free sample (~14.9 μm) indicating the restriction in grain growth of TiC. Such a phenomenon is related to the effect of WC addition as a grain growth inhibitor in TiC-based ceramics. The grain size reduction in the sintered composites could be resulted from the pinning effects of reinforcement on grain boundaries mobility due to the existence of WC. Indeed, during the sintering of TW0, the motion of grain boundaries was not hindered which contributes to grain growth. However, in WC reinforced TiC samples, the additive particles exert a pinning force on the matrix grain boundaries and causes the decrease in grain size of TW1.5 and TW3 samples. According to the Zener pinning effect [65, 66], the introduction of 3 wt% WC reinforcement in TiC

provides strong pinning effects on matrix grains and prevents the mobility of the grain boundaries at high temperatures. Moreover, Sun *et al*. [65, 66] has presented another equation for Zener factor (Z) related to the second phase particles surface area as following, in which the surface area of reinforcement particles is denoted by S_v.

$$Z = \frac{S_V}{4}$$

It is obvious that the nano-sized powder has higher surface to volume ratio; thus, it can be deduced that nano-sized WC particles create greater pinning pressure (Z) and results in exerting higher hindrance force against TiC grain growth.

Fig. 8. Average TiC grain size in the as-sintered samples versus the amount of nano-sized WC addition.

Qu *et al*. showed that WC addition into Ti(C, N)-matrix promotes the sinterability of TiC and limits the grain coarsening [67]. Guindal *et al*. investigated solid solubility of WC in TiC and determined that TiC dissolves WC at high temperatures via the substitution of Ti atoms by W atoms [29]. As shown in Fig. 9, two regions were observed by consideration of TiC-WC phase diagram, which indicates that when the TiC content is more than 73 wt% at temperatures lower than 2000 ˚C, two phases appear as (Ti,W)C and WC [29]. However, when the amount of WC is less than 73 wt%, only (Ti,W)C is formed which indicates that the dissolution and reprecipitation of WC on TiC grains can be occurred during the sintering of TiC-WC compacts at 1900 ˚C.

Fig. 9. TiC–WC phase diagram.

To identify the distribution of elements in the microstructure of sintered WC reinforced TiC matrix composite, EDS mapping analysis was performed on the TW3 sample (Fig. 10). The higher concentration of tungsten in the grain boundary areas verifies the generation of (Ti,W)C solid solution during sintering stage. The XRD analysis result for TW3 sample is presented in Fig. 11. No obvious WC peak is detected in the XRD pattern, which is due to the

small amount of WC. The generation of (Ti,W)C solid-solution is also responsible for disappearance of WC peak in the XRD patterns. It seems that the XRD peaks of TiC phase slightly move to high angels that can be attributed to dissolution of WC in matrix.

Fig. 10. FESEM micrograph of polished surface of TW3 ceramic and corresponding EDS elemental mapping.

Fig. 11. XRD pattern of the as-sintered TiC-based ceramic containing 3wt% nano-sized WC.

4. Conclusions

In this study, TiC-(0, 1.5, 3 wt%) WC ceramics were fabricated by spark plasma sintering at 1900 °C under 40 MPa pressure. The microstructural evolution and thermal-mechanical properties *e.g*. thermal conductivity, hardness and flexural strength of the prepared ceramics were investigated. The addition of 1.5wt% nano-sized WC reinforcement in TiC matrix apparently increases the porosity, while, the utilization of 3wt% nano-sized WC powder enhances the sintering driving force and leads to achieve the maximum compaction of TiC during sintering. X-ray powder diffraction and energy-dispersive X-ray analyses results showed that there is not any reaction between WC and TiC, but high solubility of WC in TiC leads to generation of (Ti,W)C solid solution at high temperatures throughout sintering process. The results also indicated that the grain growth in TiC–3wt% WC was inhibited due to the existence of WC reinforcement and formation of (Ti,W)C solid solution that exerts pinning pressure on TiC grain boundaries. Enhanced hardness and flexural strength of TiC ceramics were obtained with the addition of 3wt% WC, which could be attributed to densification improvement and fine grain size. In addition, it has been concluded that when WC content is 1.5 wt%, the sintered composite exhibits lower thermal conductivity while with the rise of WC content to 3 wt%, the thermal conductivity decreases.

References

[1] L. Cheng, Z. Xie, G. Liu, Spark plasma sintering of TiC-based composites toughened by submicron SiC particles, Ceram. Int. 39 (5) (2013) 5077–5082.

[2] Y. Gu, J. X. Liu, F. Xu, G.J. Zhang, Pressureless sintering of titanium carbide doped with boron or boron carbide, J. Eur. Ceram. Soc., 37 (2) (2017) 539-547.

[3] Z. Fu, R. Koc, Pressureless sintering of submicron titanium carbide powders, Ceram. Int. 43 (18) (2017) 17233-17237.

[4] K. S. Vecchio, J. C. Lasalvia, M. A. Meyers, G. T. Gray, Microstructural characterization of self-propagating high-temperature synthesis/ dynamically compacted and hot-pressed titanium carbides, Metallurgical Transactions A, 23 (1) (1992) 87–97.

[5] J. L. Li, L. J. Wang, G. Z. Bai, W. Jiang, Microstructure and mechanical properties of in situ produced TiC/C nanocomposite by spark plasma sintering, Scripta Materialia, 52 (9) (2005) 867-871.

[6] R. Chaim, L. Kleiner, S. Kalabukhov, Densification of nanocrystalline TiC ceramics by spark plasma sintering, Materials Chemistry and Physics, 130 (1–2) (2011) 815-821.

[7] L. Wang, W. Jiang, L. Chen, S. Bai, Rapid Reactive Synthesis and Sintering of Submicron TiC/SiC Composites through Spark Plasma Sintering, J. Am. Ceram. Soc., 87 (6) (2004) 1157–1160.

[8] L. Cheng, Z. Xie, J. Liu, H. Wu, Q. Jiang, S. Wu, Effects of Y2O3 on the densification and fracture toughness of SPS-sintered TiC, Materials Research Innovations, 22 (1) (2018) 7-12.

[9] L. Cheng, Z. Xie, G. Liu, W. Liu, W. Xue, Densification and mechanical properties of TiC by SPS-effects of holding time, sintering temperature and pressure condition, Journal of the European Ceramic Society, 32 (12) (2012) 3399-3406.

[10] J.Cabrero, F. Audubert, R. Pailler, Fabrication and characterization of sintered TiC–SiC composites, Journal of the European Ceramic Society, 31 (3) (2011) 313-320.

[11] Y. Li, H. Katsui, T. Goto, Spark plasma sintering of TiC–ZrC composites, Ceramics International, 41 (5) (2015) 7103-7108.

[12] J. Chen, W. Jun, L. W. Jiang, Characterization of sintered TiC–SiC composites, Ceramics International, 35 (8) (2009) 3125-3129.

[13] A. Teber, F. Schoenstein, F. Têtard, M. Abdellaoui, N. Jouini, Effect of SPS process sintering on the microstructure and mechanical properties of nanocrystalline TiC for tools application, International Journal of Refractory Metals and Hard Materials, 30 (1) (2012) 64-70.

[14] A. Sabahi Namini, S.N. Seyed Gogani, M. Shahedi Asl, K. Farhadi, M. Ghassemi Kakroudi, A. Mohammadzadeh, Microstructural development and mechanical properties of hot pressed SiC reinforced TiB2 based composite, Int. J. Refract. Met. Hard Mater. 51 (2015) 169–179.

[15] M. Shahedi Asl, A. Sabahi Namini, M. Ghassemi Kakroudi, Influence of silicon carbide addition on the microstructural development of hot pressed zirconium and titanium diborides, Ceram. Int. 42 (4) (2016) 5375–5381.

[16] K. Farhadi, A. Sabahi Namini, M. Shahedi Asl, A. Mohammadzadeh, M. Ghassemi Kakroudi, Characterization of hot pressed SiC whisker reinforced TiB2 based composites, Int. J. Refract. Met. Hard Mater. 61 (2016) 84–90.

[17] A. Sabahi Namini, M. Azadbeh, M. Shahedi Asl, Effect of TiB2 content on the characteristics of spark plasma sintered Ti–TiBw composites, Advanced Powder Technology, 28 (2017) 1564–1572.

[18] T. Ishigaki, K. Sato, Y. Moriyoshi, Pressureless sintering of TiC–Al2O3 composites. J Mater Sci Lett. 8 (1989) 678–680.

[19] M. Sribalaji, B. Mukherjee, A. Islam, A. Kumar Keshri, Microstructural and mechanical behavior of spark plasma sintered titanium carbide with hybrid reinforcement of tungsten carbide and carbon nanotubes, Materials Science and Engineering A, 702 (15) (2017) 10-21.

[20] H. Xiong, Z. Li, K. Zhou, TiC whisker reinforced ultra-fine TiC-based cermets: Microstructure and mechanical properties, Ceramics International, 42 (6) (2016) 6858-6867.

[21] K. Vasanthakumar, S. R. Bakshi, Effect of C/Ti ratio on densification, microstructure and mechanical properties of TiCx prepared by reactive spark plasma sintering, Ceramics International, 44 (1) (2018) 484-494.

[22] Y. Li, H. Katsui, T. Goto, Spark plasma sintering of TiC–ZrC composites, Ceramics International, 41 (5) (2015) 7103-7108.

[23] G. Liua, Z. Yang, J. Li, G. He, Y. Chen, K. Chen, D. Fan, Reaction path in formation of Ti1−xWxC solid solution by combustion synthesis, Ceramics International, 44 (6) (2018) 6127-6136.

[24] V. K. Vitryanyuk, F. I. Chaplygin, G. D. Kostenetskaya, Properties of complex TiC-WC carbides in their homogeneity region, Soviet Powder Metallurgy and Metal Ceramics, 10 (7) (1971) 547–552.

[25] L. Cheng, Z. Xie, G. Liu, Spark plasma sintering of TiC ceramic with tungsten carbide as a sintering additive, Journal of the European Ceramic Society, 33 (15–16) (2013) 2971-2977.

[26] J. Jung, S. Kang, Sintered (Ti,W)C carbides, Scripta Materialia, 56 (7) (2007) 561-564.

[27] H. C. Kim, D. K. Kim, K. D. Woo, I. Y. Ko, I. J. Shon, Consolidation of binderless WC–TiC by high frequency induction heating sintering, International Journal of Refractory Metals and Hard Materials, 26 (1) (2008) 48-54.

[28] M. Yang, Z. Guo, J. Xiong, F. Liu, K. Qi, Microstructural changes of (Ti,W)C solid solution induced by ball milling, International Journal of Refractory Metals and Hard Materials, 66 (2017) 83-87.

[29] M. J. M. Guindal, L. Contreras, X. Turrillas, G. B. M. Vaughan, Å. Kvick, M. A. Rodríguez, Self-propagating high-temperature synthesis of TiC–WC composite materials, Journal of Alloys and Compounds, 419 (1–2) (2006) 227-233.

[30] I. J. Shon, Mechanical properties and rapid sintering of binderless nanostructured TiC and WC by high frequency induction heated sintering, Journal of Ceramic Processing Research, 17 (7) (2016) 707-711.

[31] B. Haldar, D. Bandyopadhyay, R. C. Sharma, N. Chakraborti, The Ti-W-C (Titanium-Tungsten-Carbon) System, Journal of Phase Equilibria, 20 (3) (1999) 337–343.

[32] H. Abderrazak, F. Schoenstein, M. Abdellaoui, N. Jouini, Spark plasma sintering consolidation of nanostructured TiC prepared by mechanical alloying, International Journal of Refractory Metals and Hard Materials, 29 (2) (2011) 170-176.

[33] M. Akhlaghi, S.A. Tayebifard, E. Salahi, M. Shahedi Asl, Spark plasma sintering of TiAl–Ti3AlC2 composite, Ceramics International, (2018) doi:10.1016/j.ceramint.2018.08.272.

[34] M. Dashti Germi, Z. Hamidzadeh Mahaseni, Z. Ahmadi, M. Shahedi Asl, Phase evolution during spark plasma sintering of novel Si3N4-doped TiB2–SiC composite, Materials Characterization, 145 (2018) 225– 232.

[35] Y. Azizian-Kalandaragh, A. Sabahi Namini, Z. Ahmadi, M. Shahedi Asl, Reinforcing effects of SiC whiskers and carbon nanoparticles in spark plasma sintered ZrB2 matrix composites, Ceramics International, 44 (16) (2018) 19932– 19938.

[36] E. Ghasali, M. Shahedi Asl, Microstructural development during spark plasma sintering of ZrB2–SiC–Ti composite, Ceramics International, 44 (15) (2018) 18078–18083.

[37] M. Shahedi Asl, B. Nayebi, Z. Ahmadi, S. Parvizi, M. Shokouhimehr, A novel ZrB2–VB2–ZrC composite fabricated by reactive spark plasma sintering, Materials Science and Engineering: A, 731 (2018) 131–139.

[38] M. Shahedi Asl, B. Nayebi, M. Shokouhimehr, TEM characterization of spark plasma sintered ZrB2–SiC–graphene nanocomposite, Ceramics International, 44 (13) (2018) 15269–15273.

[39] Z. Hamidzadeh Mahaseni, M. Dashti Germi, Z. Ahmadi, M. Shahedi Asl, Microstructural investigation of spark plasma sintered TiB2 ceramics with Si3N4 addition, Ceramics International, 44 (11) (2018) 13367–13372.

[40] Z. Ahmadi, B. Nayebi, M. Shahedi Asl, I. Farahbakhsh, Z. Balak, Densification improvement of spark plasma sintered TiB2-based composites with micron-, submicron- and nano-sized SiC particulates, Ceramics International, 44 (10) (2018) 11431–11437.

[41] S. Parvizi, Z. Ahmadi, M. Jaberi Zamharir, M. Shahedi Asl, Synergistic effects of graphite nano-flakes and submicron SiC particles on the characteristics of spark plasma sintered ZrB2 nanocomposites, International Journal of Refractory Metals and Hard Materials, 75 (2018) 10–17.

[42] M. Shahedi Asl, B. Nayebi, Z. Ahmadi, M. Jaberi Zamharir, M. Shokouhimehr, Effects of carbon additives on the properties of ZrB2–based composites: A review, Ceramics International, 44 (7) (2018) 7334–7348.

[43] A. Sabahi Namini, M. Azadbeh, M. Shahedi Asl, Effects of in-situ formed TiB whiskers on microstructure and mechanical properties of spark plasma sintered Ti–B4C and Ti–TiB2 composites, Scientia Iranica, 25 (2) (2018) 762–771.

[44] M. Shahedi Asl, A statistical approach towards processing optimization of ZrB2–SiC–graphite nanocomposites. Part I: Relative density, Ceramics International, 44 (6) (2018) 6935– 6939.

[45] M. Shahedi Asl, M. Jaberi Zamharir, Z. Ahmadi, S. Parvizi, Effects of nano-graphite content on the characteristics of spark plasma sintered ZrB2–SiC composites, Materials Science and Engineering: A, 716 (2018) 99–106.

[46] M. Shahedi Asl, A. Sabahi Namini, A. Motallebzadeh, M. Azadbeh, Effects of sintering temperature on microstructure and mechanical properties of spark plasma sintered titanium, Materials Chemistry and Physics, 203 (2018) 226–273.

[47] M. Shahedi Asl, Microstructure, hardness and fracture toughness of spark plasma sintered ZrB2–SiC–Cf composites, Ceramics International, 43 (17) (2017) 15047–15052.

[48] M. Shahedi Asl, Z. Ahmadi, S. Parvizi, Z. Balak, I. Farahbakhsh, Contribution of SiC particle size and spark plasma sintering conditions on grain growth and hardness of TiB2 composites, Ceramics International, 43 (16) (2017) 13924–13931.

[49] Z. Balak, M. Azizieh, H. Kafashan, M. Shahedi Asl, Z. Ahmadi, Optimization of effective parameters on thermal shock resistance of ZrB2-SiC-based composites prepared by SPS: Using Taguchi design, Materials Chemistry and Physic, 196 (2017) 333–340.

[50] Z. Balak, M. Shahedi Asl, M. Azizieh, H. Kafashan and R. Hayati, Effect of different additives and open porosity on fracture toughness of ZrB2–SiC-based composites prepared by SPS, Ceramics International, 43 (2017) 2209–2220.

[51] I. Farahbakhsh, Z. Ahmadi, M. Shahedi Asl, Densification, microstructure and mechanical properties of hot pressed ZrB2–SiC ceramic doped with nano-sized carbon black, Ceramics International, 43 (11) (2017) 8411–8417.

[52] Z. Ahmadi, B. Nayebi, M. Shahedi Asl, M. Ghassemi Kakroudi and I. Farahbakhsh, Sintering behavior of ZrB2–SiC composites doped with Si3N4: A fractographical approach, Ceramics International, 43 (13) (2017) 9699–9708.

[53] M. Shahedi Asl, M. Ghassemi Kakroudi, I. Farahbakhsh, B. Mazinani and Z. Balak, Synergetic effects of SiC and Csf in ZrB2-based ceramic composites. Part II: Grain growth, Ceramics International, 42 (2016) 18612–18619.

[54] B. Nayebi, M. Shahedi Asl, M. Ghassemi Kakroudi, I. Farahbakhsh and M. Shokouhimehr, Interfacial phenomena and formation of nano-particles in porous ZrB2–40 vol% B4C UHTC, Ceramics International, 42 (2016) 17009–17015.

[55] M. Shahedi Asl, F. Golmohammadi, M. Ghassemi Kakroudi and M. Shokouhimehr, Synergetic effects of SiC and Csf in ZrB2-based ceramic composites. Part I: Densification behavior, Ceramics International, 42 (3) (2016) 4498–4506.

[56] B. Nayebi, M. Shahedi Asl, M. Ghassemi Kakroudi and M. Shokouhimehr, Temperature dependence of microstructure evolution during hot pressing of ZrB2–30 vol% SiC composites, International Journal of Refractory Metals and Hard Materials, 54 (2016) 7–13.

[57] M. Shahedi Asl, I. Farahbakhsh and B. Nayebi, Characteristics of multi-walled carbon nanotube toughened ZrB2–SiC ceramic composite prepared by hot pressing, Ceramics International, 42 (1) (2016) 1950–1958.

[58] Z. Ahmadi, B. Nayebi, M. Shahedi Asl and M. Ghassemi Kakroudi, Fractographical characterization of hot pressed and pressureless sintered AlN-doped ZrB2–SiC composites, Materials Characterization, 110 (2015) 77–85.

[59] M. Shahedi Asl, M. Ghassemi Kakroudi, F. Golestani-Fard and H. Nasiri, A Taguchi approach to the influence of hot pressing parameters and SiC content on the sinterability of ZrB2-based composites,International Journal of Refractory Metals and Hard Materials, 51 (2015) 81–90.

[60] M. Shahedi Asl, B. Nayebi, Z. Ahmadi, P. Pirmohammadi and M. Ghassemi Kakroudi, Fractographical characterization of hot pressed and pressureless sintered SiAlON-doped ZrB2–SiC composites, Materials Characterization, 102 (2015)137–145.

[61] M. Shahedi Asl and M. Ghassemi Kakroudi, A processing–microstructure correlation in ZrB2–SiC composites hot-pressed under a load of 10 MPa, Universal Journal of Materials Science, 3 (2015). 14–21.

[62] A. Babapoor, M. Shahedi Asl, Z. Ahmadi, A. Sabahi Namini, Effects of spark plasma sintering temperature on densification, hardness and thermal conductivity of titanium carbide, Ceramics International, 44 (2018) 14541–14546.

[63] Z. Z. Lin, C. L. Huang, D. C. Luo, Y. H. Feng, X. X. Zhang, G. Wang, Thermal performance of metallic nanoparticles in air, Appl. Therm. Eng. 105 (2016) 686–690.

[64] M. Patel, V.V.B. Prasad, V. Jayaram, Heat conduction mechanisms in hot pressed ZrB2 and ZrB2–SiC composites, J. Eur. Ceram. Soc. 33 (10) (2013) 1615–1624.

[65] M. Miodownik, E.A. Holm, G.N. Hassold, Highly parallel computer simulations of particle pinning: zener vindicated, Scr. Mater. 42 (2000) 1173–1177.

[66] N. Sun, B.R. Patterson, J.P. Suni, H. Weiland, L.F. Allard, Characterisation of particle pinning potential, Acta Mater. 15 (15) (2006) 4091–4099.

[67] Qu J, Xiong WH, Ye DM, Yao ZH, Liu WJ, Lin SJ. Effect of WC content on the microstructure and mechanical properties of Ti(C0.5N0.5)–WC–Mo–Ni cermets. Int J Refract Met Hard Mater. 28 (2010) 243–249.

Table 1. The design of compositions for TiC-WC samples.

Sample name	WC (wt%)
TW0	0
TW1.5	1.5
TW3	3

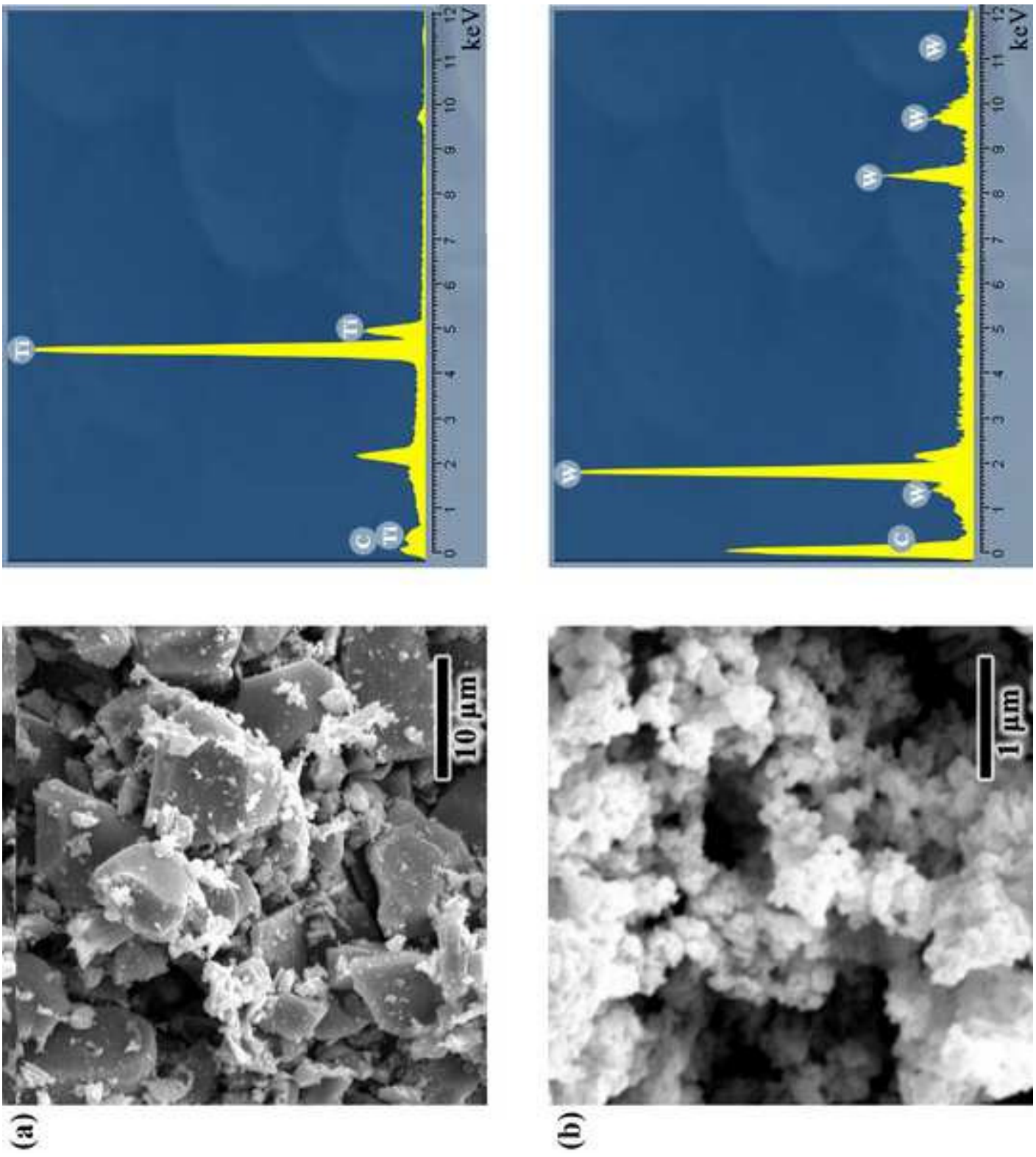

Figure 1

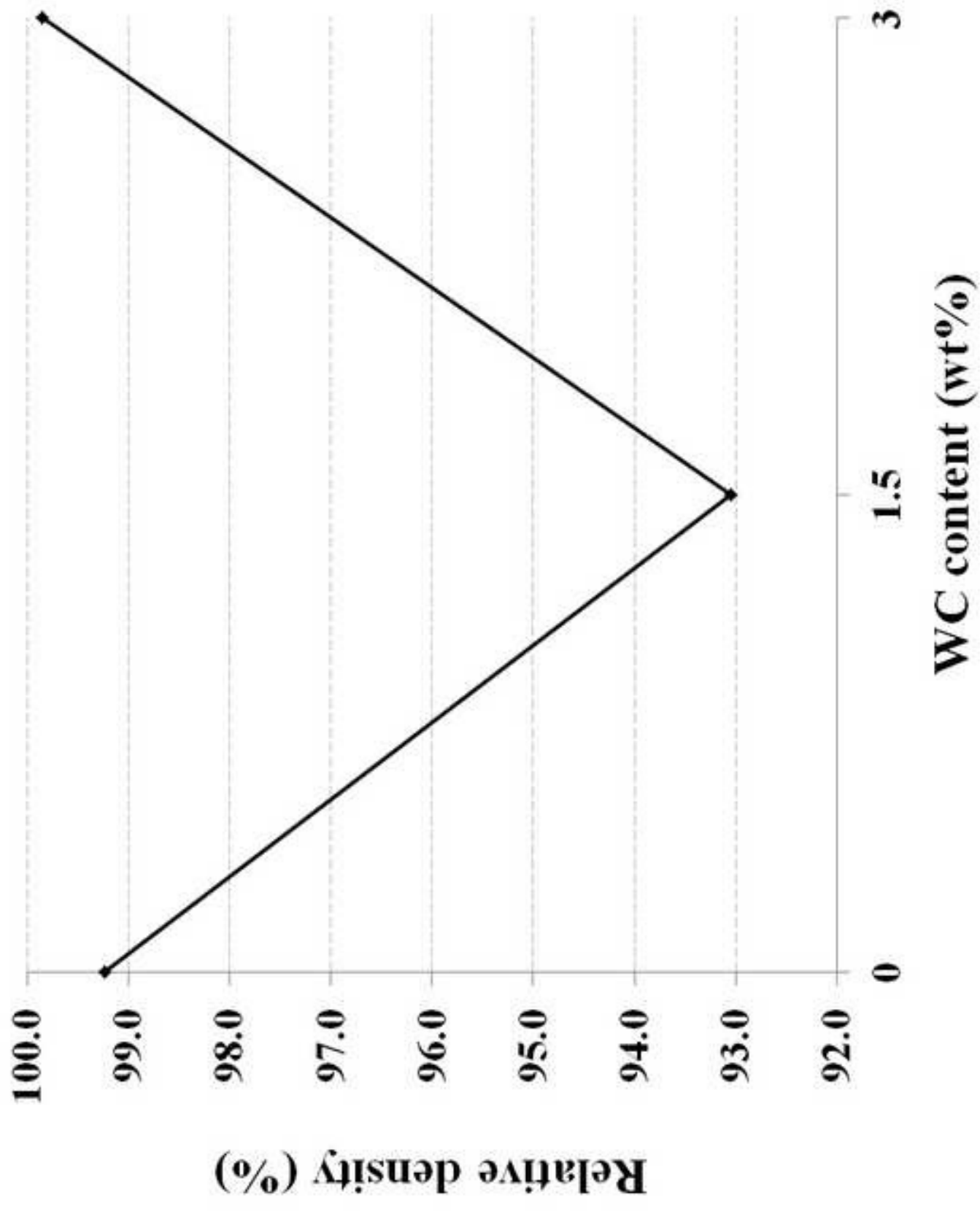

Figure 2

Figure 3

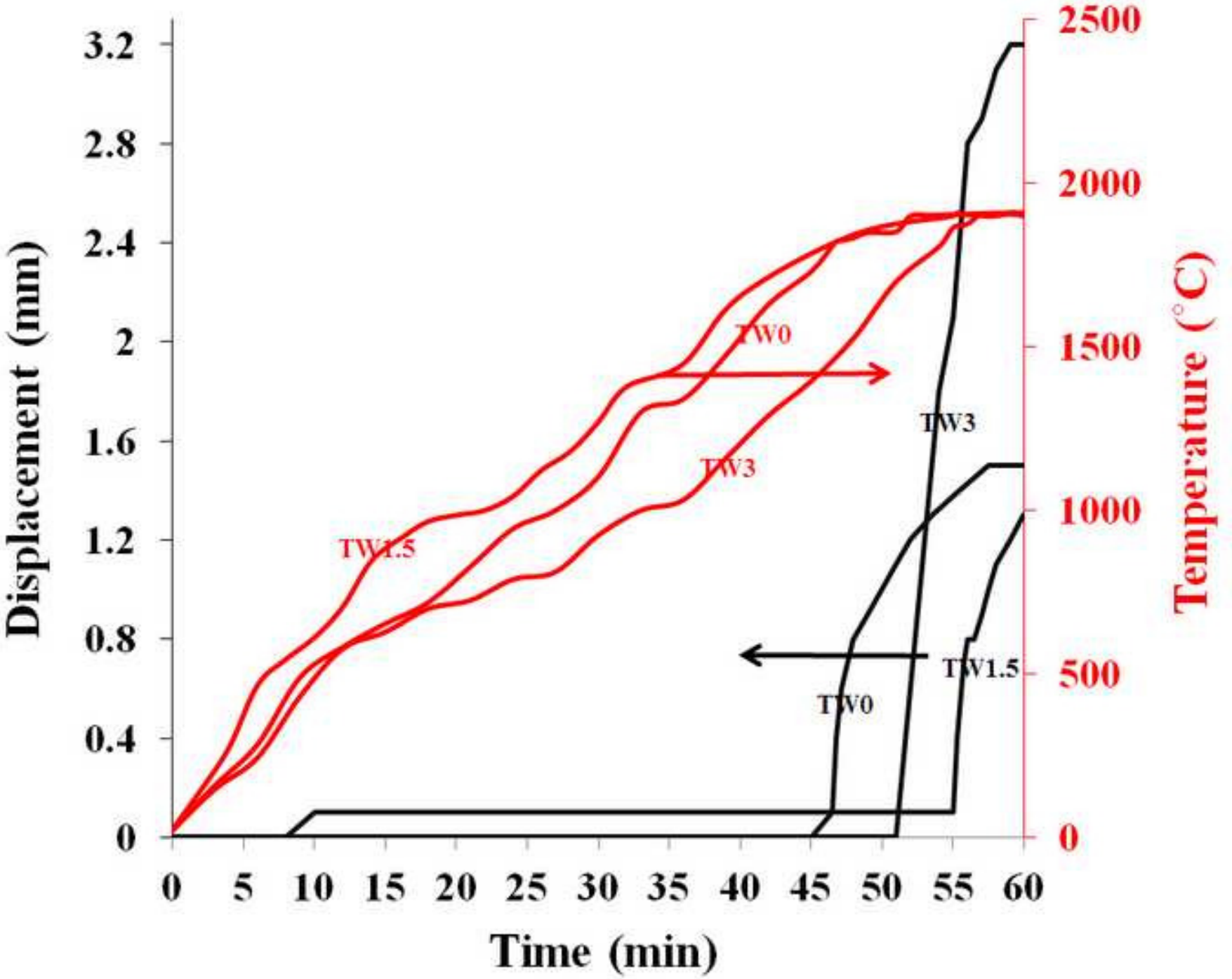

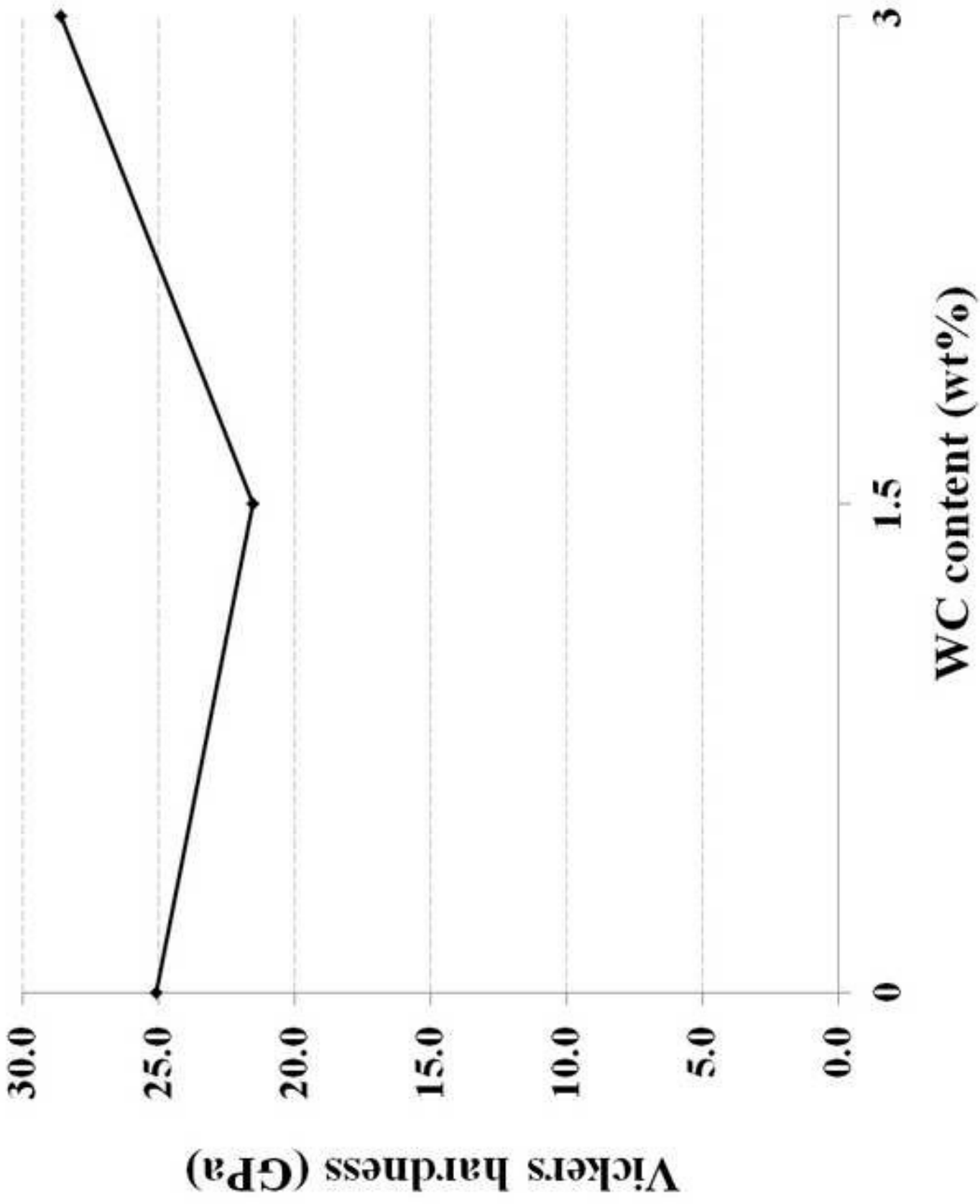

Figure 4

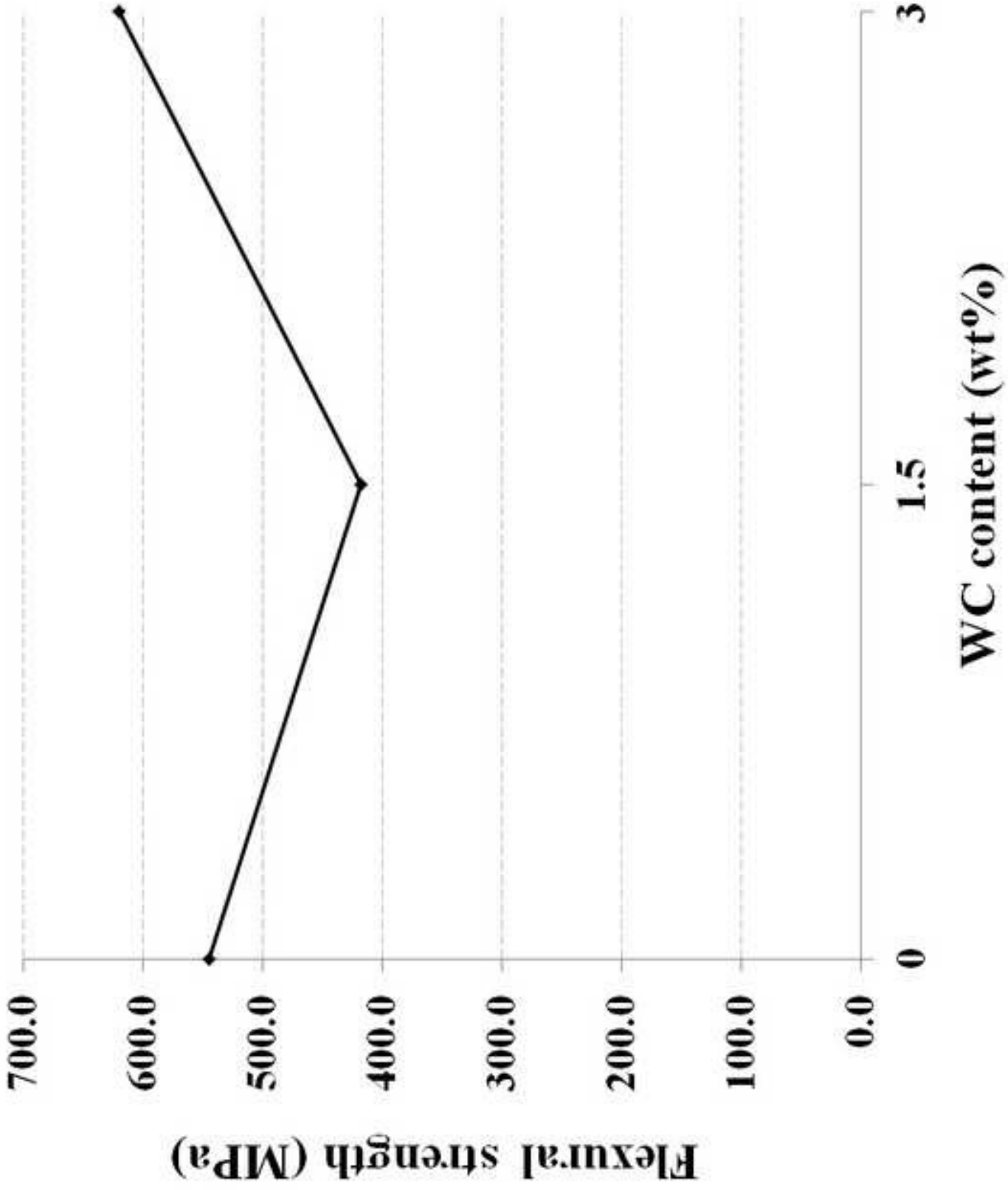
Flexural strength (MPa)
700.0
600.0
500.0
400.0
300.0
200.0
100.0
0.0
0
1.5
3
WC content (wt%)

Figure 5

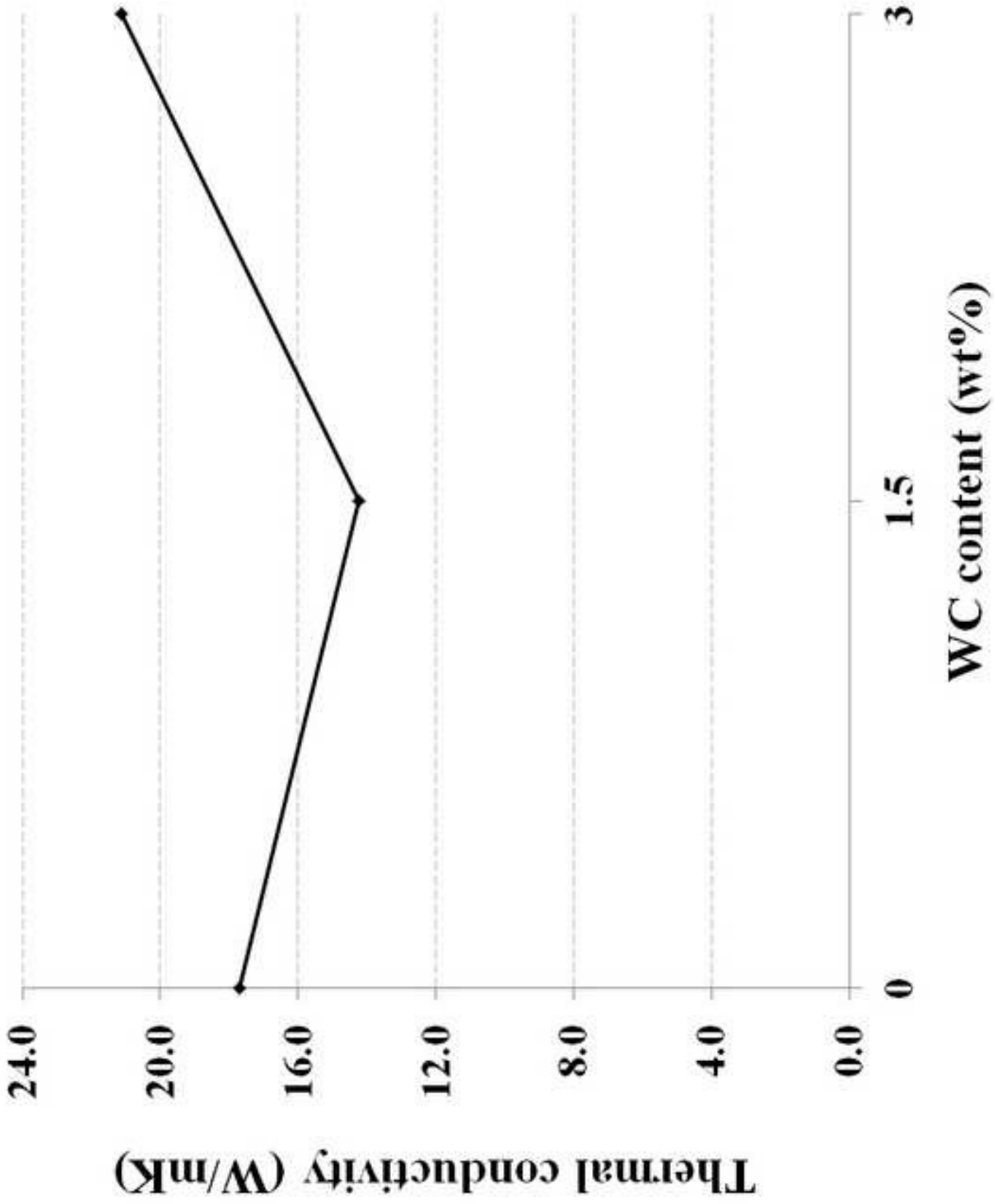
Thermal conductivity (W/mK)
24.0
20.0
16.0
12.0
8.0
4.0
0.0
0
1.5
3
WC content (wt%)

Figure 6

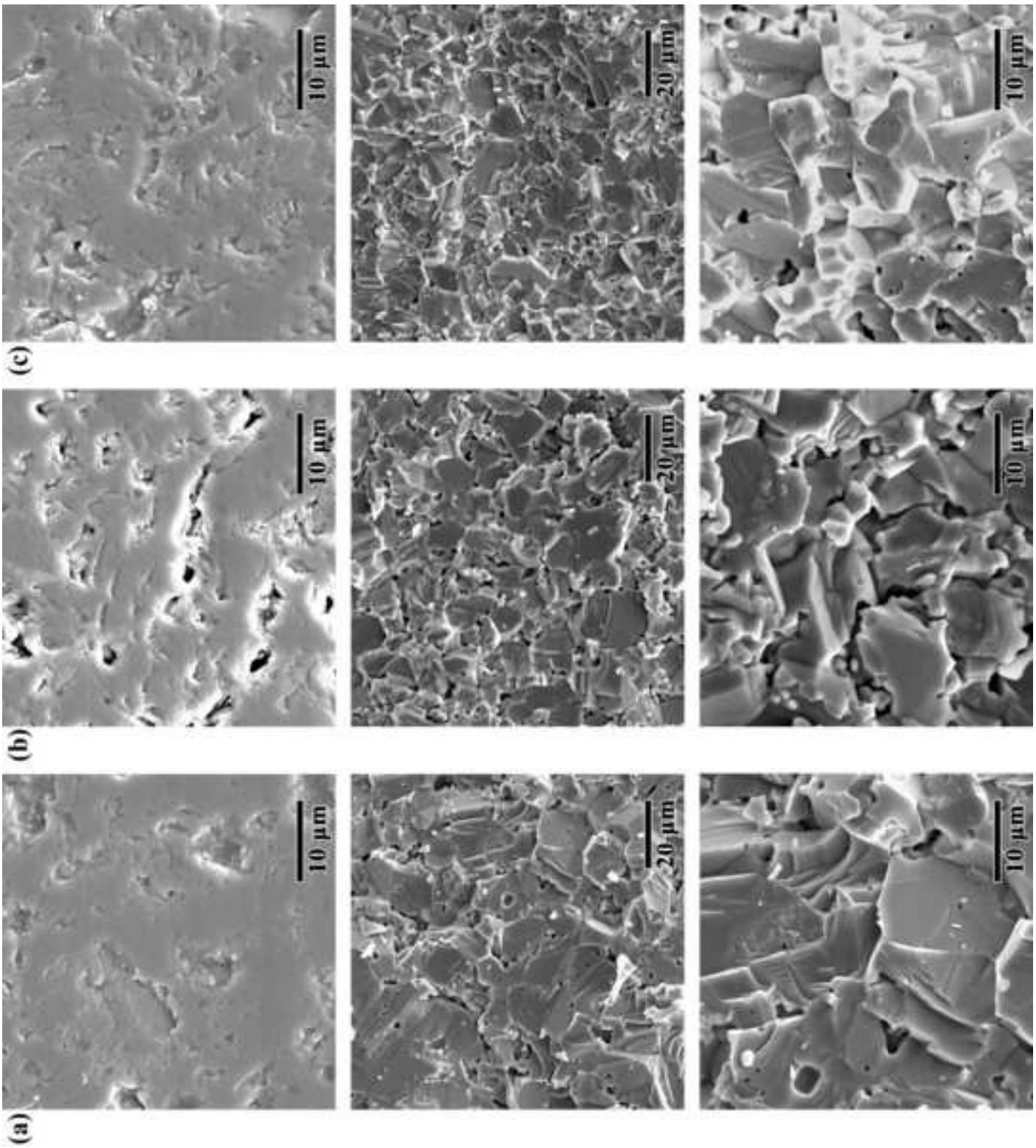

Figure 7

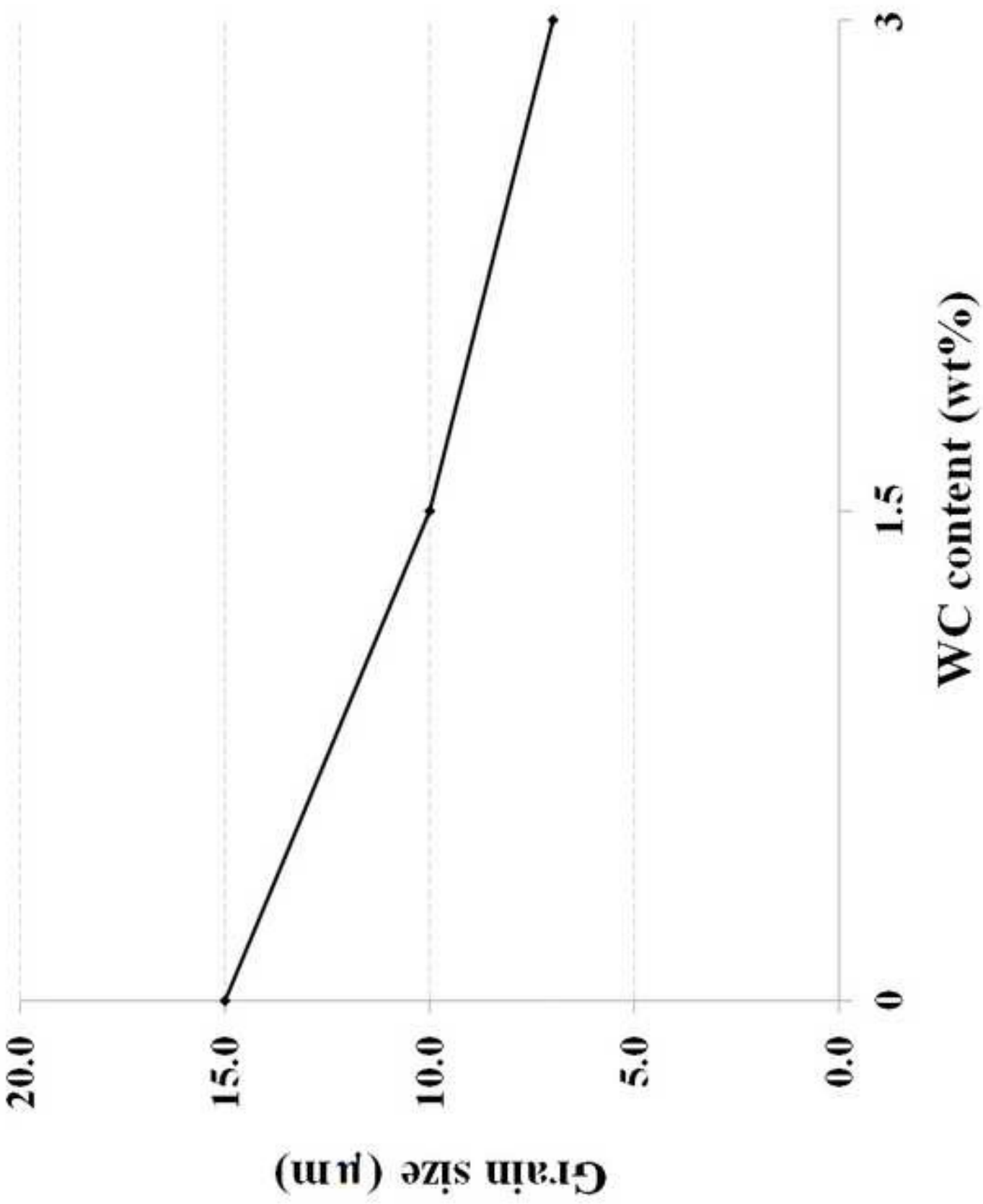

Figure 8

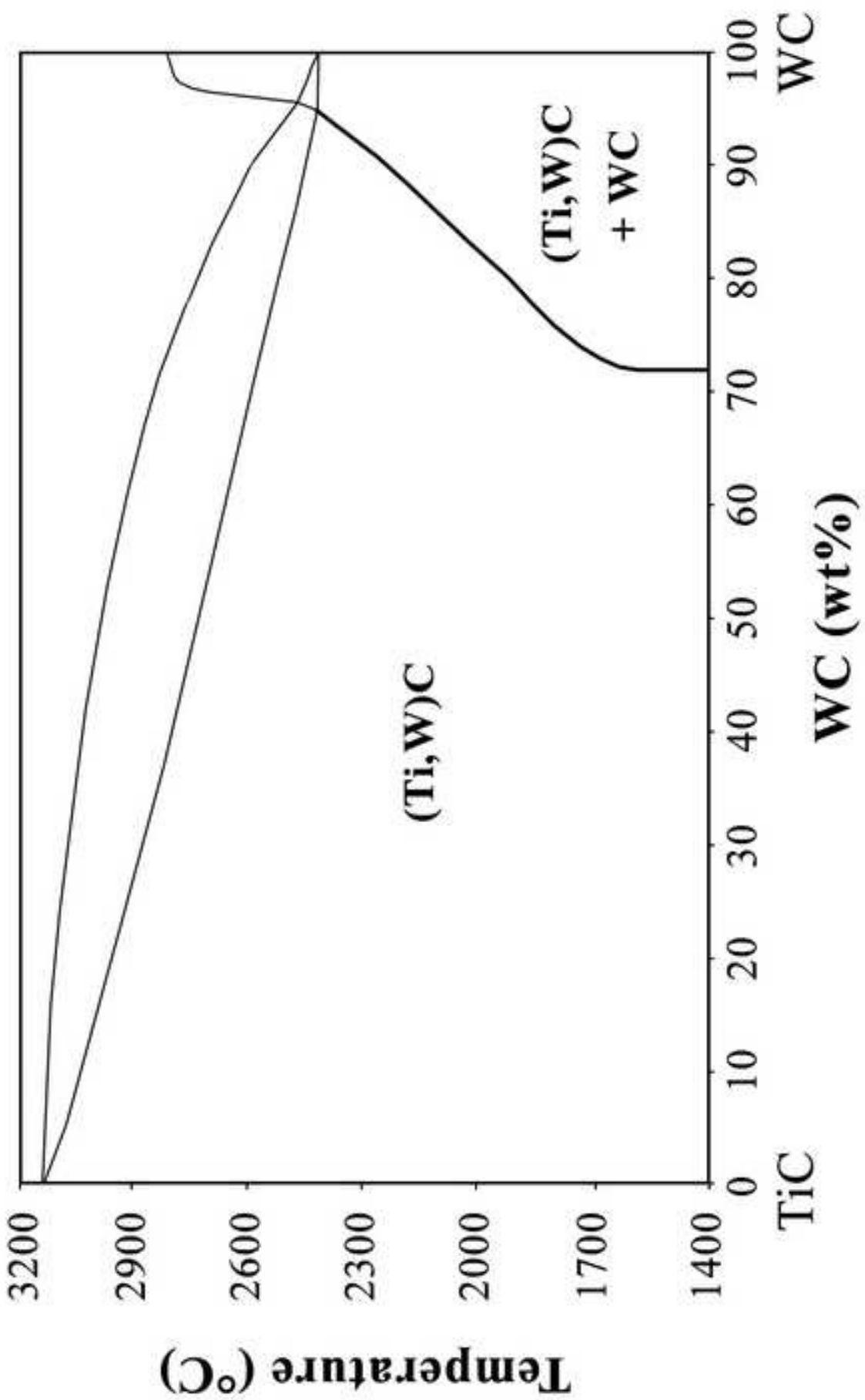

Figure 9

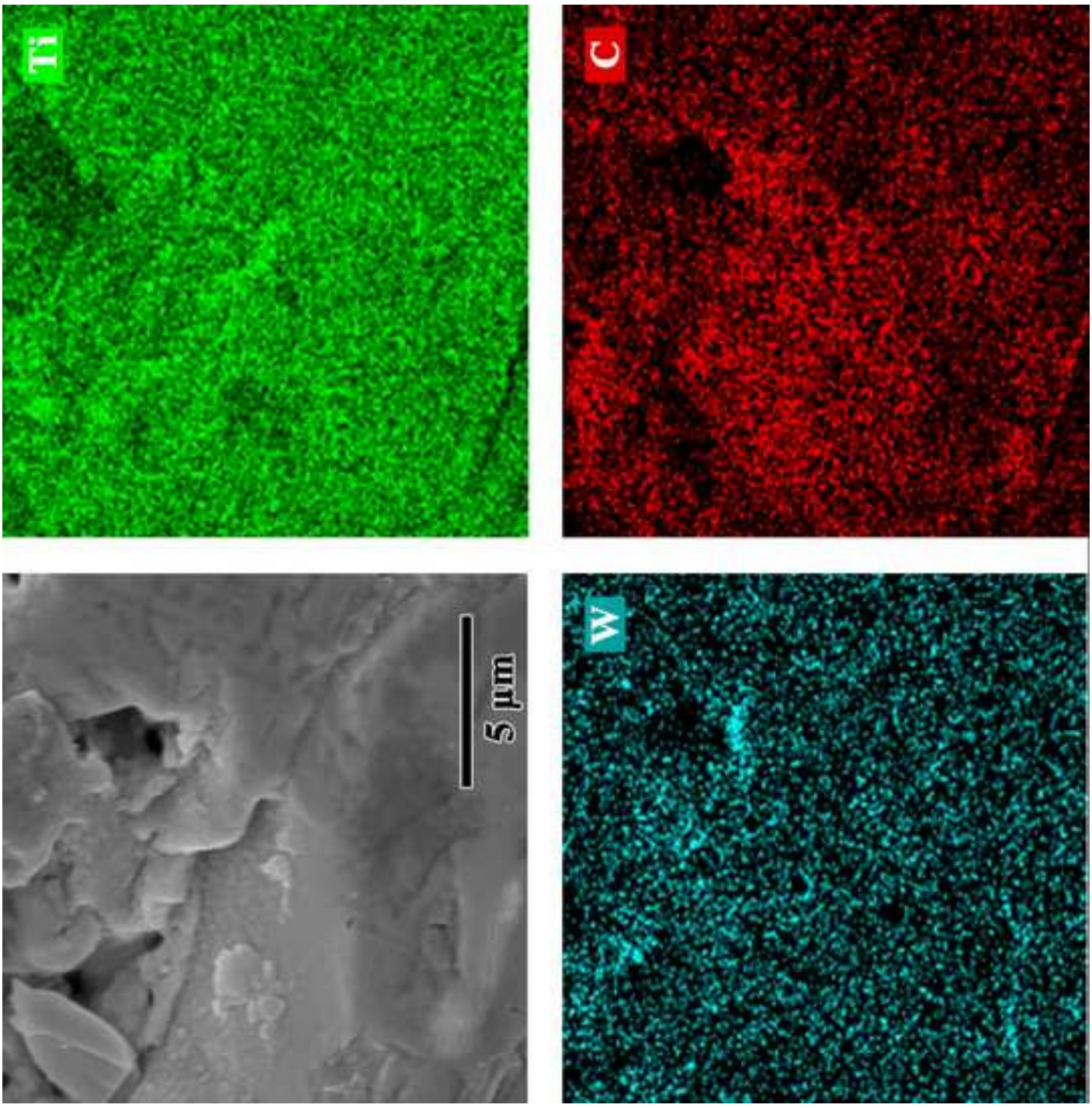

Figure 10

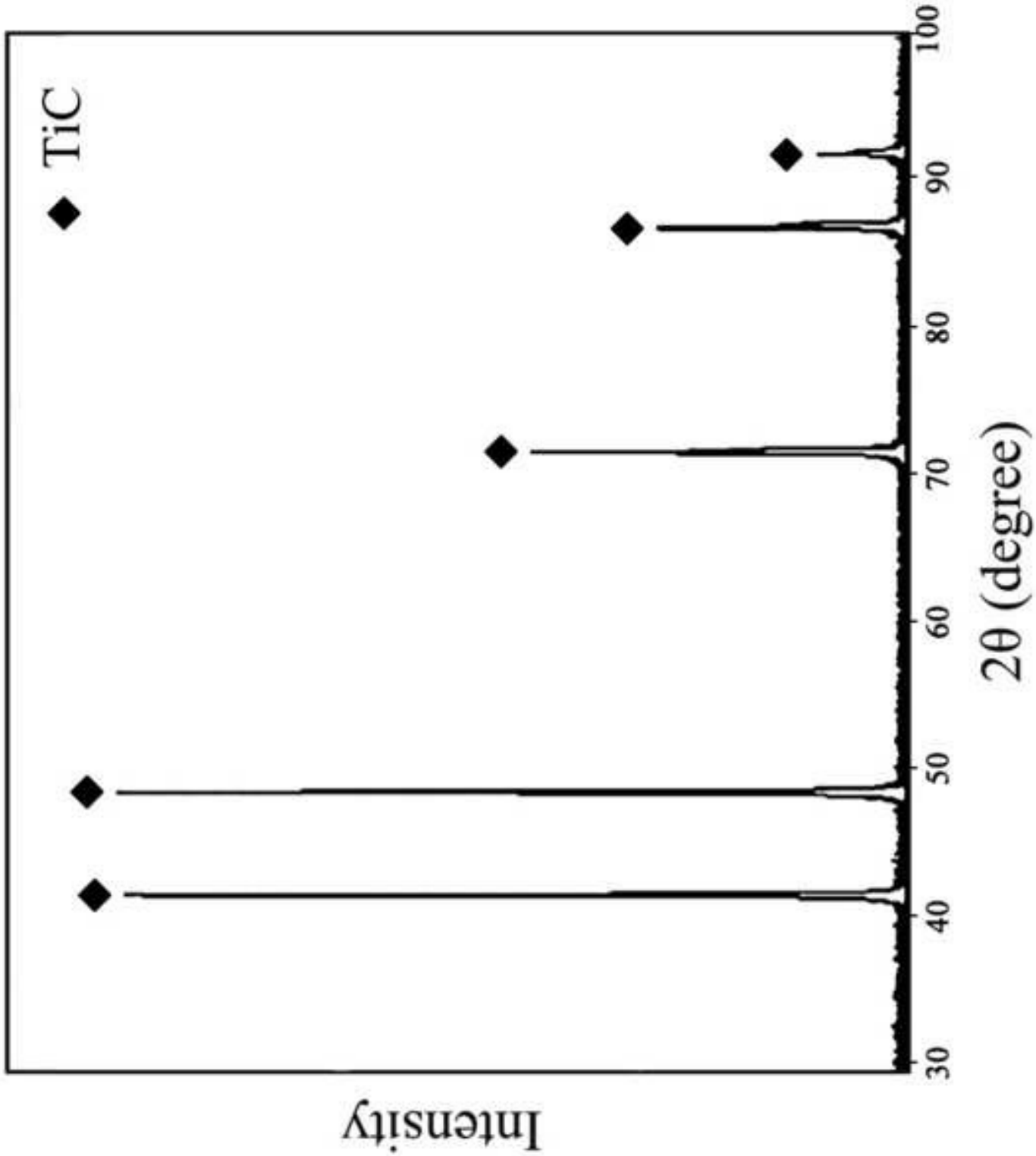

Figure 11